

UPGRADE ON THE EXPERIMENTAL ACTIVITIES FOR ESS AT THE LASA VERTICAL TEST FACILITY

M. Bertucci*, A. Bosotti, A. D'Ambros, P. Michelato, L. Monaco, C. Pagani¹,
R. Paparella, D. Sertore, INFN/LASA, Segrate (MI), Italy
¹also Università degli Studi di Milano, Milano, Italy

Abstract

The LASA vertical test facility is equipped for the cold test of ESS medium-beta 704.42 MHz cavities, with and without He tank, and is integrated with several diagnostic tools allowing a careful analysis of cavity performance limitations. This paper reports the latest tests on ESS cavities - both prototypes and series - and a discussion on the experimental results. The recent instrumental upgrades implemented in the facility - and the ones foreseen for the future in view of a further improvement of cavity performances - are also pointed out.

INTRODUCTION

The series production cavities of the medium beta section of ESS are tested after the tank integration at the DESY AMTF facility, which allows the validation of two cavities at a time [1]. The time evolution of the cooldown procedure at AMTF is very similar to the one typically used for cryomodules. Cavities can be let 12 h at 100 K to test possible Q-disease effects and there is also the possibility of performing a fast cooldown from 100 K to 4.2 K.

However, some of the series cavities along the production may exhibit an irregular behavior (geometrical defects on surface, welding imperfections, pitting,...) that would deserve a careful control before the tank integration. For instance, if some defect on cavity inner surface is noticed by the optical inspection, there is the risk of a premature thermal breakdown mechanism occurring before the ESS qualification values for Q and accelerating field are reached. In these cases, a more in-depth vertical cold test procedure could give useful information about how to recover a possible performance limitation. Aiming to do this, we upgraded the vertical test facility at INFN-LASA for the test of ESS 704.42 MHz medium beta cavities. In summary, LASA vertical test facility allows to test the ESS cavities at different temperatures (up to 1.6 K) with dedicated diagnostic tools. A first description of LASA facility is presented in [2] and [3].

We report here briefly a general description of the facility and deepen the most recent upgrades and the foreseen infrastructure modifications that will be undertaken in order to improve the cavity performances.

THE VERTICAL TEST FACILITY

The LASA vertical cryostat is shown in Fig. 1 on the left. Its diameter is 0.7 m and can host cavities with frequencies

≥ 500 MHz. The connections of the cryostat vacuum system subcooling pumps can be seen coming out from the cover and then on the bunker wall. All signal cables are connected to the top flange of the insert. After the cavity is inserted inside, the cryostat is pumped down to high vacuum so to perform a leak check before the helium transfer.



Figure 1: Left: upper part the vertical cryostat. Right: top view of the cryostat internal surface.

Cryogenic operation starts with filling the cryostat with liquid helium, transferred from 450 liter dewars. In order to reach a liquid He level 20 cm above the cavity top flange, 2300 liters has to be transferred inside the cryostat. This grants at least 8 hours of RF measurements at 2 K. The cooldown rate is approximately 0.5 K min^{-1} when crossing the critical temperature $T_c = 9.2 \text{ K}$.

Also visible in Fig. 1 is the mu-metal magnetic shield, which surrounds the cryostat and reduces the absolute value of the residual magnetic field to $< 8 \text{ mG}$ in the cavity region. The residual magnetic field inside cryostat has been mapped by means of a triaxial fluxgate magnetometer in the position corresponding to the cavity. Figure 2 shows the value of magnetic field magnitude as function of depth, in 4 different angles at the position of cavity equators.

The cavity is fed by a 650 W UHF power amplifier. The power is coupled to the cavity by a coaxial antenna (High Q Antenna) of nominal $Q_I = 10^{10}$. We choose to limit the amplifier output power to 250 W, as a redundant safety margin, being this power more than enough to our test purposes. To sample the cavity transmitted power, a pick-up antenna ($Q_{ext} = 3 \cdot 10^{11}$) is installed on the cavity beam tube opposite to the main coupler. Transmitted power signal is then extracted from the cryostat through high screened cryogenic coaxial cables. The cavity accelerating field E_{acc} and the

* michele.bertucci@mi.infn.it

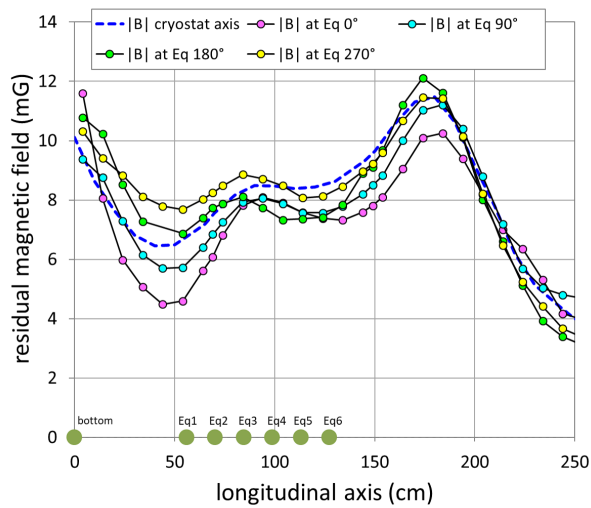


Figure 2: Magnetic field magnitude inside the LASA cryostat. 0 point correspond to cryostat bottom. Green dots mark the position of ESS medium beta cavity equators.

quality factor Q_0 are measured by the accurate reading of the input (P_i), reflected (P_r), and transmitted (P_t) power both in CW and pulsed mode. The cavity transmitted and reflected power are demodulated, when in transient mode, so to get the (loaded) discharge time. This allows the calculation of the input port coupling factor β_i , then the evaluation of cavity Q_0 at low field, and the determination of the calibration constant that allows the calculation of E_{acc} from P_t during the power rise. Due to its high Q_0 and hence very tight bandwidth (less than 1 Hz), the cavity must be inserted in a Phase Locked Loop (PLL) to be tested. All the readout instrumentation is interfaced to a LabVIEW control program that also allows to set the pulse timings and the calibration constants for correct signal readouts. The program allows to acquire data for the different measurement sections (R_s vs. T, power rises) [4]. A block diagram of the cavity measurement system is shown in Fig. 3.

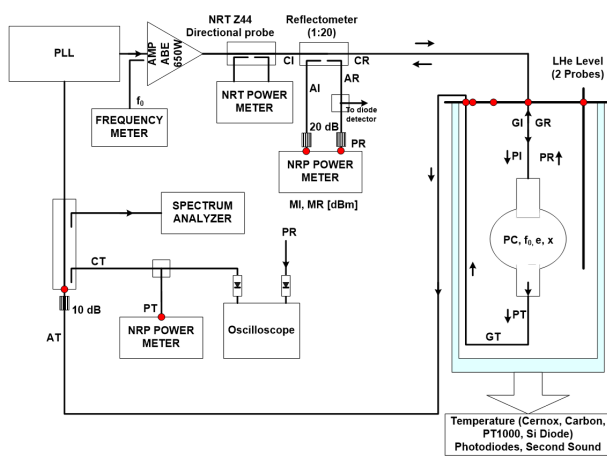


Figure 3: Diagram of the RF system used for the ESS cavity test.

Cavity Diagnostics

The cavity diagnostics setup has been extensively described in [3]. In brief, thermal breakdown events are detected by means of fast thermometry and second sound. Cernox and CCS fast-thermometry sensors are placed in proximity of critical zones. Other thermal sensors (also PT100s and PT1000s) are placed in the cryostat to monitor its thermal behavior during cooldown. In addition, a Lakeshore DT-670 silicon diode temperature sensor is employed to follow the cooling down of the cavities. The Second Sound system for the 3D mapping of the cavity quenches consist of 20 OST installed on the frame surrounding the cavity.

ESS medium beta cavities revealed to be particularly prone to field emission events. Therefore we intensified our efforts to have a more wide understanding of the dynamics of field emission and the subsequent X-ray generation. External radiation dose is continuously measured every second by means of a proportional counter (Thermo Electron FH 40-G), which can measure doses up to 1 Sv h^{-1} but has poor sensitivity for X-ray energies higher than 1.3 MeV. For this reason a NaI(Tl) scintillator detector (Ortec 905-3) is also employed, with the purpose of covering the high energy zone of radiation and to measure the X-ray spectrum. The spectra are continuously acquired every second and registered by means of a dedicated VI developed in LabVIEW. In this way the spectrum end-point (i.e. the electron impact energy) can be calculated as function of instantaneous accelerating field.

The external dose and spectrum measurement can offer only a partial reconstruction of what is occurring inside the cryostat. The radiation generated on cavity surface by means of electron Bremsstrahlung undergoes a series of interactions and attenuation processes which also depend on the impact energy (for instance, above 8 MeV nuclear reactions triggering neutron production can also occur). As an attempt of numerically reconstruct the energy transfer from an internal source to an external radiation detector, figure 4 shows the calculation performed by means of FLUKA of the energy deposition of an electron source (10 MeV , 10^7 electrons per second, corresponding to a $1.6 \cdot 10^{-5} \text{ J}$ per second) hitting the cavity beam tube flange. The internal structure of the cryostat is reconstructed and a detector equivalent volume (NaI) is placed at its true position outside the cryostat cover. According to these simulations, $2 \cdot 10^{-8} \text{ J}$ are adsorbed per second without Pb screening, that would result in complete detector saturation, and $2 \cdot 10^{-11} \text{ J}$ per second by assuming 10 cm of Pb screening. This means that detector is experiencing the total energy reduced by a factor 10^6 .

The internal radiation is measured by means of an array of 28 photodiodes (Hamamatsu S6775), uniformly distributed around the cavity irises and beam tubes. Amplifier boards are placed nearby the diode so to minimize pick-up noise from cables. All the electronics is suitable in the cryogenic context (CMOS based op-amps, metal film capacitors,...). The signals are extracted from cryostat, collected by a NI DAQ unit and registered by a LabVIEW VI.

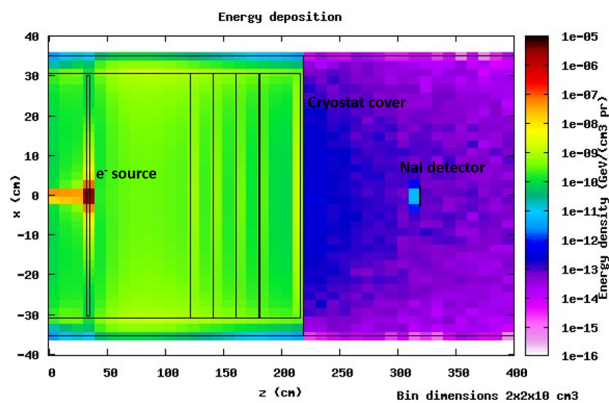


Figure 4: Energy deposition generated by 10^7 electrons at 10 MeV hitting cavity beam tube flange.

Figure 5 shows a ESS medium beta cavity mounted on the vertical insert with all diagnostics installed. On the right, the details of a OST and a photodiode sensor are shown.

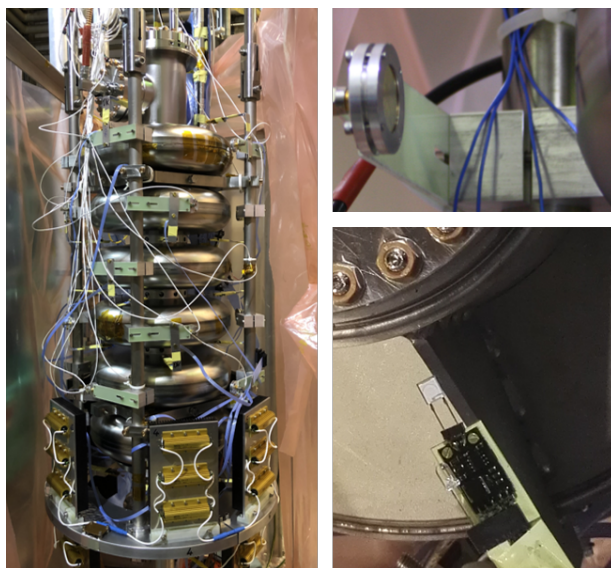


Figure 5: Left: a ESS cavity fully equipped with diagnostics. Top right: OST sensor (detail). Bottom right: photodiode sensor at top beam tube flange (detail).

Plan for Future Infrastructure Upgrades

In view of forthcoming LASA-INFN activities for PIP-II, aiming at reaching higher Q w.r.t ESS, we are planning a series of infrastructure upgrades, whose purpose is to minimize the trapped flux contribution to the residual resistance. When working with low frequency cavity, like 650 MHz of PIP-II low beta section and 704.42 MHz of ESS medium beta section, the residual resistance term overwhelms the BCS contribution, already at 2 K. The goal of a Q-improvement therefore requires a reduction of the residual magnetic field and an increase of the cooldown rate.

A cylindrical cryoperm shield is under procurement. It is expected to be placed inside the cryostat and it will be

concentric with the existing one that is installed outside the vessel. Magnetostatic calculations indicate a reduction of magnetic field to less than the half of current value by employing this double-shield configuration. A complete compensation of remnant longitudinal field component might be achieved through Helmholtz coils around the cavity. Such solution is now under study.

From the cooldown rate side, we are currently limited to 0.5 K min^{-1} . A fluxgate sensor is installed on cavity surface for monitor the flux expulsion at 9.2 K, but no jump at 9.2 K in the response of fluxgate has been so far observed. From measures of Cernox sensors installed in correspondence of cavity top and bottom sides, the thermal gradient at the transition is only 0.5 K m^{-1} . An increase of both this parameters is necessary for minimize the flux trapping sensitivity [5]. Aiming to obtain this, the cryostat and the process lines will be redesigned in order to allow for a short transient of high mass flow and gas throughput.

Besides improving the cooldown dynamics, we are studying a new configuration for the cryostat pumping elements and the vacuum chain so to push the power limits for cavity CW operation at 2 K from the current value of 40 W up to 70 W, and a direct line for cryostat filling at 2 K that will allow to extend the cavity testing time [6].

VERTICAL TEST OF CAVITY M006

As an example, we present here the case of cavity M006. In this instance, some suspect features appeared on the inner cavity surface after the bulk BCP treatment. Fig. 6 shows the image acquired with the optical inspection device at equator 6, angle 260° . Several defects, of mm size, are clearly visible near the welding. As reported in [7], these defects are pits with a depth of the order of 0.1 mm, so it has been impossible to remove them even after several hours of mechanical grinding.

Given the high risk of poor cavity performance, we decided to test the cavity without tank at LASA vertical test facility, so to exploit all the available diagnostic tools for understanding the limiting mechanisms in case of premature cavity quench.

Vertical Test Results

The cavity surface resistance $R_s(T) = R_{BCS}(T) + R_0$ has been measured during the cooldown. SUPERFIT code [8] has been employed to separate the $R_{BCS}(T)$ (BCS resistance) and R_{res} (residual resistance) contributions. Reduced band gap $\frac{\Delta}{k_B T_c}$, electron mean free path l_e and residual resistance R_0 were treated as free parameters, while $T_c = 9.25 \text{ K}$, $\lambda_l = 32 \text{ nm}$ and $\xi_0 = 39 \text{ nm}$ were used as fixed parameters for critical temperature, London penetration depth and coherence length, respectively. The result of the fit is shown in Fig. 7. Fitted values for reduced bandgap, electron mean free path and residual resistance are shown in the insert. Assuming the worst case scenario of complete flux trapping and a typical value of $S \approx 0.25 \text{ n}\Omega \text{ mG}^{-1}$ for sensitivity to trapped

Content from this work may be used under the terms of the CC BY 3.0 licence (© 2019). Any distribution of this work must maintain attribution to the author(s), title of the work, publisher, and DOI.

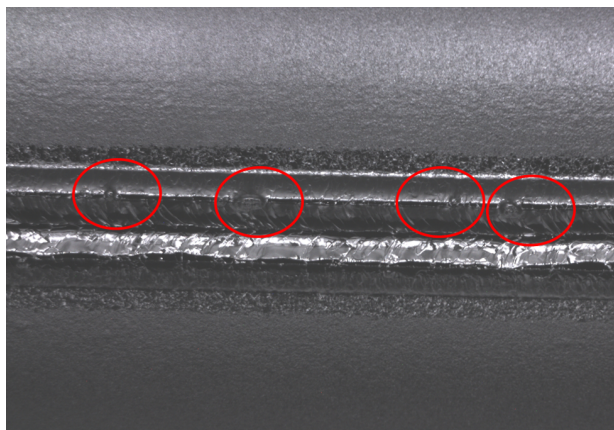


Figure 6: Image of cavity M006 inner surface after bulk BCP and heat treatment.

flux of 700 MHz cavities at low field [9], the residual field of 8 mG contributes with only 2 nΩ to residual resistance.

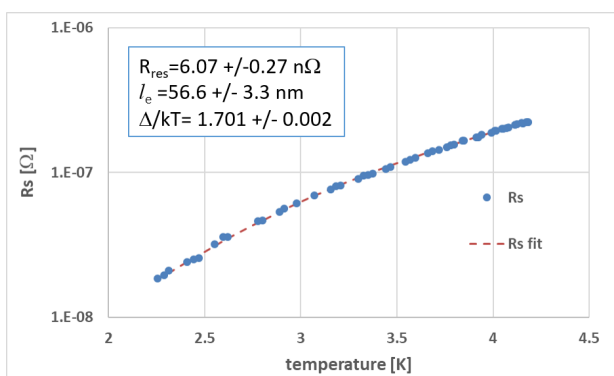


Figure 7: Measured and fitted surface resistance as function of bath temperature.

The first cavity test at 2 K is reported on the top graph of Fig. 8. A premature drop of Q value takes place starting from 7 MV m⁻¹, accompanied by a sudden rise of radiation. A maximum value of 23 mSv h⁻¹ has been reached at around 10-11 MV m⁻¹. At the same field level, the Q₀ reaches its minimum value of 3.8 · 10⁹. The trend changes when the field is increased further. Radiation level decreases and Q₀ rises again. Eventually cavity quenches at the maximum field of 17.9 MV m⁻¹ with a Q₀ = 1 · 10¹⁰ and a moderate radiation level of 2 mSv h⁻¹.

A conditioning procedure for the cavity has been then performed, by keeping its field level at 9 MV m⁻¹ for 1 hour, and then the test has been repeated. The bottom graph of 8 shows the results of the test after conditioning. Now, the Q vs E_{acc} curve displays a more straightforward behavior, but the quench field level and Q-value at quench are unchanged. Now, two separate zones of field emission can be noticed.

- A multipacting barrier appears in the 9-11 MV m⁻¹ interval. Multipacting at the same field level has been already noticed in the prototype tests [10], in agreement with the result of simulations performed with FishPACT

code [11]. The radiation level is moderate (less than 0.1 mSv h⁻¹)

- X-ray radiation starts at around 13 MV m⁻¹ and reach a maximum value of ≈ 2 mSv h⁻¹ at the quench field of 17.9 MV m⁻¹, following the typical dependence of Fowler-Nordheim Law. The dose level at quench field is very close to the value measured before conditioning.

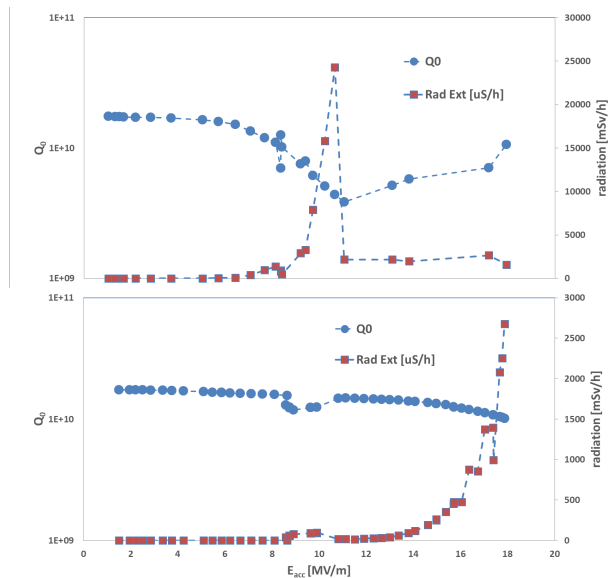


Figure 8: Plot of Q₀ vs E_{acc} and radiation vs E_{acc} for the first vertical test of cavity M006 (top) and after conditioning (bottom).

Results From Cavity Diagnostics

Figure 9 shows the photodiode readout during the power rise. During the multipacting barrier crossing, sensors iris1-0° and iris2-270° produce the highest signals. This means that main impact point for electrons generated by MP is on iris 2. Weaker signals detected by other sensors are due to secondary radiation generated by impact on cryostat walls through Compton scattering. At higher fields, the stronger signals come from iris3-270° and iris4-90° sensors. This means that the origin of X-ray radiation in the two cases (MP and high field FE) is from different points of cavity inner surface.

The X-ray spectrum has been continuously acquired during the test with the scintillator detector. Figure 10 shows the energy end-point evolution as function of time when crossing the multipacting barrier, compared with the instantaneous value of accelerating field. As for the proportional counter, radiation starts to be detected at around 9 MV m⁻¹ near the MP barrier. It is worth to notice that end-point energy nearly doubles its value (from 1 to 2 MeV while crossing the barrier, with the acc. field slightly increasing from 9 to 11 MV m⁻¹). In the next future, a model for simulating the impact energy of electron emitted at the suspected location will be implemented.

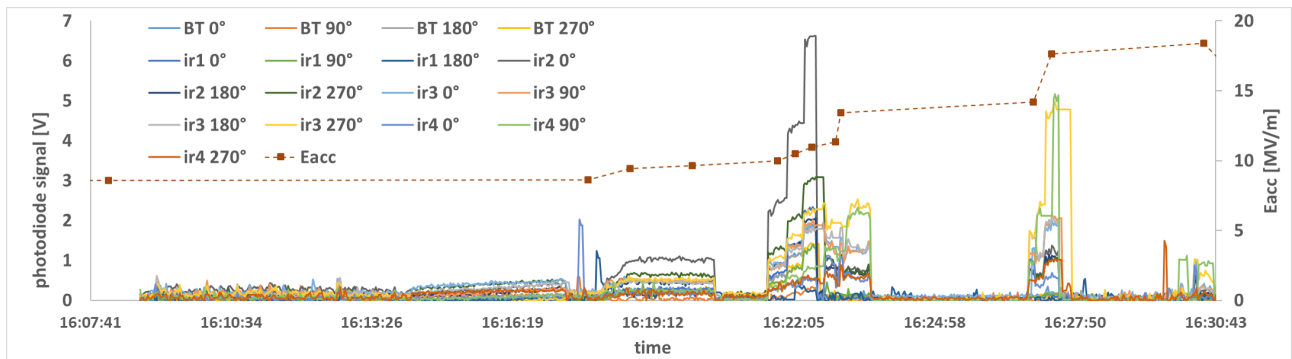


Figure 9: Photodiodes readout during the M006 power rise. The accelerating field versus time is also reported.

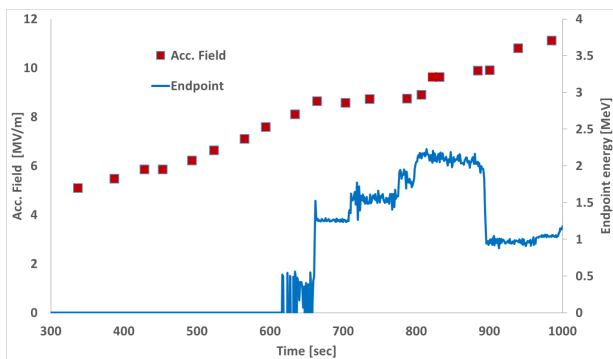


Figure 10: Plot of Energy end-point [MeV] and accelerating field [MV m^{-1}] as function of time.

Second sound has been acquired at the breakdown field. The reconstruction by trilateration algorithm confirmed the surface region shown in Fig. 6 as the origin of quench. Due to the limited 10 mm resolution of second sound technique, it is not possible to distinguish which one of the defects marked in red is the one triggering the thermal breakdown. The quench is not likely to be generated by field emission heating because the signals of photodiodes near the hot spot (namely the one installed on upper beam tube and iris 1) are low with respect to the one coming from iris 3 and 4. However, field emission occurs at the same time of thermal breakdown generated by the defects in cell 6.

CONCLUSIONS

The INFN-LASA facility for the cold test of ESS medium-beta cavities is here described. Such infrastructure allows to test cavities with and without tank, and is equipped with several diagnostic tools for monitoring field emission and thermal breakdown events. Cavity M006, which displayed some surface defect after the BCP treatment, has been tested in this facility before the tank integration so to check any possible performance limitation. The cavity actually displayed high levels of field emission and quenched at a field lower than the average value of series production [4], but above the specification value of ESS medium beta cavities.

After the conditioning procedure, the level of radiation at the nominal field of 16.9 MV m^{-1} reduced to the moderate

value of 1.5 mSv h^{-1} . Being this intermediate acceptance test successfully passed, the cavity has been inserted again inside the production cycle. The final test at DESY's AMTF facility for the cavity with tank is foreseen in the following weeks.

In the mean time, cavity M013 is expected to be tested at LASA facility in order to check the quality of the heat treatment of the recently re-qualified furnace at Zanon S.p.A. and the prototype large grain cavity MB003LG is foreseen to be tested for the first time by the early September.

REFERENCES

- [1] P. Michelato *et al.*, “Status of the ESS Medium Beta Cavities at INFN - LASA”, in *Proc. 10th Int. Particle Accelerator Conf. (IPAC'19)*, Melbourne, Australia, May 2019, pp. 2211–2214.
- [2] A. Bosotti *et al.*, “Vertical Tests of ESS Medium Beta Prototype Cavities at LASA”, in *Proc. 8th Int. Particle Accelerator Conf. (IPAC'17)*, Copenhagen, Denmark, May 2017, pp. 1015–1018. doi : 10.18429/JACoW-IPAC2017-MOPVA063
- [3] M. Bertucci *et al.*, “Quench and Field Emission Diagnostics for the ESS Medium-Beta Prototypes Vertical Tests at LASA”, in *Proc. 8th Int. Particle Accelerator Conf. (IPAC'17)*, Copenhagen, Denmark, May 2017, pp. 1007–1010. doi : 10.18429/JACoW-IPAC2017-MOPVA061
- [4] A. Bosotti *et al.*, “Vertical Test of ESS Medium Beta Cavities”, in *Proc. 10th Int. Particle Accelerator Conf. (IPAC'19)*, Melbourne, Australia, May 2019, pp. 2852–2855.
- [5] S. Posen *et al.*, “Magnetic Flux Expulsion Studies in Niobium SRF Cavities”, in *Proc. 7th Int. Particle Accelerator Conf. (IPAC'16)*, Busan, Korea, May 2016, pp. 2277–2279. doi : 10.18429/JACoW-IPAC2016-WEPMR009
- [6] R. Paparella *et al.*, “INFN-LASA for the PIP-II Project”, presented at the 19th Int. Conf. RF Superconductivity (SRF'19), Dresden, Germany, Jun.-Jul. 2019, paper MOP060, this conference.
- [7] M. Bertucci *et al.*, “Surface Treatments for the Series Production of ESS Medium Beta Cavities”, presented at the 19th Int. Conf. RF Superconductivity (SRF'19), Dresden, Germany, Jun.-Jul. 2019, paper MOP056, this conference.
- [8] G. Ciovati, “SUPERFIT: a Computer Code to fit Surface Resistance and Penetration Depth of a Superconductor”, Tech Rep. TN-003, Jlab, 2003.

Content from this work may be used under the terms of the CC BY 3.0 licence (© 2019). Any distribution of this work must maintain attribution to the author(s), title of the work, publisher, and DOI.

- [9] M. Checchin *et al.*, “Frequency Dependence of the Trapped Flux Sensitivity in SRF Cavities”, *Appl. Phys. Lett.*, vol. 112, p. 072601, 2017. doi:10.18429/JACoW-SRF2017-TUPB048
- [10] D. Sertore *et al.*, “INFN- LASA Medium Beta Cavity Prototypes for ESS Linac”, in *Proc. 18th Int. Conf. RF Superconductivity (SRF'17)*, Lanzhou, China, Jul. 2017, pp. 494–498.
- [11] J. F. Chen *et al.*, “Multipacting Study in INFN-LASA ESS Medium-Beta Cavity”, in *Proc. 8th Int. Particle Accelerator Conf. (IPAC'17)*, Copenhagen, Denmark, May 2017, pp. 1019–1022. doi:10.18429/JACoW-IPAC2017-MOPVA064